Growth of isotopically enriched ZnO nanorods of excellent optical quality

Ciarán Gray[1,*], Joseph Cullen[2], Conor Byrne[3], Greg Hughes[3], Irina Buyanova[2], Weimin Chen[2], Martin O. Henry[1], Enda McGlynn[1,*]

[1] *School of Physical Sciences, National Centre for Plasma Science and Technology, Dublin City University, Glasnevin, Dublin 9, Ireland.*

[2] *Department of Physics, Chemistry and Biology, Linköping University, S-581 83, Linköping, Sweden.*

[3] *School of Physical Sciences, Dublin City University, Glasnevin, Dublin 9, Ireland.*

*Authors to whom correspondence should be addressed: ciaran.gray5@mail.dcu.ie (Ph. 0035317007695), enda.mcglynn@dcu.ie.

ABSTRACT

We have produced isotopically enriched ZnO nanorods using Zn-enriched ZnO source powder by vapour phase transport on silicon substrates buffer-coated with unenriched ZnO seed layers. SEM and XRD data confirm successful growth of high quality, dense, *c*-axis aligned nanorods over a substantial surface area. Raman data show a shift of >1 cm^{-1} in the peak position of the Raman scattered peaks due to the E_2^{low} and E_2^{high} phonon modes when the Zn isotope is changed from ^{64}Zn to ^{68}Zn, consistent with previous work, thus confirming successful isotopic enrichment. SIMS data provides additional confirmation of enrichment. The optical quality (as determined by photoluminescence feature intensity and linewidth) is excellent. Samples with Zn isotopic enrichment ranging from ^{64}ZnO to ^{68}ZnO display a shift in recombination energy of the bound excitons at the band edge (3.34 - 3.37 eV) of ~ 0.6 meV. This blue shift is also consistent with previously published data, further confirming

both the excellent optical quality and successful isotopic substitution of ZnO nanorods using this relatively simple growth method.

KEYWORDS

A1. Characterization, A1. Nanostructures, A2. Growth from vapour, B1. Zinc compounds, B2. Semiconducting II-VI materials.

1. INTRODUCTION

Nanostructures of ZnO have received much interest in the research literature over the past decade and have been produced in many morphologies including thin films[1], nanorods, nanowires[2–5], nanowalls[6], nanodisks[7], nanohelixes, nanosprings, nanorings, nanobelts[8] and nanobowls.[9] One area of particular interest has being the production of ZnO nanorods for use in optical applications and studies. These have been produced using a number of growth methods including chemical bath deposition (CBD), vapour phase transport, chemical vapour deposition (CVD) and hydrothermal deposition.[2,3,5,10–13] Furthermore, isotopic enrichment is a very useful technique in the study of crystal structure and impurities in semiconductor materials such as ZnO, and comparable materials including Si, GaN and GaP, particularly using optical methods.[14–19] Reports using isotopically enriched ZnO samples have included studies of bandgap energies, phonon positions and linewidths and heat capacity, but in all cases using bulk single crystal samples with quite poor optical quality.[20–23] In this work, we report a relatively fast, easy and reliable method of producing Zn-isotopically enriched ZnO nanorods of very high structural quality, as well as excellent optical quality as determined by low temperature photoluminescence (PL) studies,

requiring small quantities of source materials. The natural isotopic abundance in ZnO is 48.6% ^{64}ZnO, 27.9% ^{66}ZnO, 4.1% ^{67}ZnO, 18.8% ^{68}ZnO and 0.6% ^{70}ZnO.[20] Natural ZnO therefore has an average atomic mass of $^{65.4}$ZnO. In this study we have grown ZnO samples enriched with ^{64}Zn, ^{66}Zn and ^{68}Zn, as well as samples with engineered isotopic abundances.

2. MATERIALS AND METHODS

The growth method used is a three step process involving the deposition of a buffer layer of ZnO nanorods using drop coating and chemical bath deposition (CBD), followed by the main growth of the nanorods using carbothermal reduction vapour phase transport (VPT). CBD, VPT and carbothermal reduction VPT are common methods used to grow ZnO nanorods.[2,5,10,11,24] The growth method used here was developed in our group and was based upon other work both in our group and reports in the literature.[2,3,25] It is further modified in this work. The growth method yields material with excellent optical quality (in terms of both emission intensity and spectral linewidths), which allow high resolution PL investigations to be carried out. The growth method is also quick and relatively easy to carry out.

The ZnO nanorods were grown on silicon (100) substrates typically 1-4 cm^2 in size. The silicon was cleaned by sonication in acetone followed by ethanol and dried in a nitrogen stream. No attempt was made to remove the native oxide layer. In the first stage of the growth process, the seed layer was deposited by drop coating 3.75 μL of 0.005 M zinc acetate in absolute ethanol solution per cm^2 of sample area to the substrate. This droplet was left for 20 seconds before being rinsed off the surface with copious amounts of fresh ethanol. This process was repeated four more times for each sample. The substrates were then annealed at 350 °C in air for 30 minutes to decompose the zinc salt into zinc oxide. This process

produces a thin layer of crystallographically aligned ZnO crystallites on the surface which act as nucleation sites for nanorod growth at later stages.

The second phase of the growth process is the deposition of a buffer layer of ZnO nanorods on the silicon substrate by CBD. A 0.02 M zinc nitrate solution was then slowly added to an equal volume of 0.8 M NaOH solution while stirring vigorously. The mixture was heated to approximately 70 °C and stirred gently. The sample was then submerged in the solution for 25 minutes while the temperature is maintained at 70 °C and the solution stirred gently. The sample was then removed, washed with copious amounts of DI-H_2O and dried with a gentle nitrogen stream. This process leaves a layer of *c*-axis textured ZnO nanorods which acts as a buffer layer for subsequent growth of larger nanorods using VPT. Neither the seed nor buffer layers are isotopically enriched; they have the natural Zn isotope abundances.

The third stage in the growth of ZnO nanorods is carbothermal reduction VPT. 10 mg of ZnO powder and 10 mg of graphite powder were carefully mixed to produce a fine homogeneous powder mixture. This powder was then spread over a length of about 2 cm in an alumina boat. The silicon wafer was suspended above the powder with the ZnO buffer layer facing downwards towards the powder. The alumina boat was then placed into a quartz tube (inner diameter 37 mm) in a single temperature zone horizontal tube furnace. The quartz tube was purged with an Ar flow of 90 sccm for about 5-10 minutes. The temperature was then increased to 925 ˚C for 1 hour with the Ar flow remaining at 90 sccm. The furnace was then allowed to cool for several hours. When the temperature reached about 350 °C, the Ar flow was stopped and the alumina boat removed. This results in the growth of ZnO nanorods aligned with their *c*-axes normal to the substrate.

Isotopically enriched ZnO nanorod samples were grown by substituting the natural ZnO powder with Zn-enriched ZnO powders. Samples of ^{64}ZnO, ^{66}ZnO and ^{68}ZnO were grown as well as samples with equal proportions of two different isotopes using 5 mg of each

powder along with 10 mg of graphite ($^{64/66}$ZnO, $^{66/68}$ZnO and $^{64/68}$ZnO). Similarly, a sample containing three different Zn isotopes was produced using 3 mg of each powder along with 10 mg of graphite ($^{64/66/68}$ZnO). The Zn isotopically enriched material in this study was enriched to 99.9% for ^{64}ZnO, 99.3% for ^{66}ZnO and 99.3% for ^{68}ZnO (Isoflex). The oxygen was in its natural isotopic abundance state (i.e. 99.76% ^{16}O).

The samples were characterised using scanning electron microscopy (SEM; Karl-Zeiss EVO series), x-ray diffraction (XRD; Bruker AXS D8 Advance Texture Diffractometer), secondary ion mass spectroscopy (SIMS), Raman spectroscopy and low temperature PL. Secondary ion mass spectroscopy (SIMS) analysis was performed in an ultra-high vacuum (UHV) system with a base pressure of $1x10^{-9}$ mbar. The SIMS setup included a Hiden Analytical IG20 ion gun operating with a positive argon ion beam of 5 KeV at a chamber partial pressure of $5x10^{-5}$ mbar 99.99% purity argon with the analysis chamber not exceeding $2x10^{-8}$ mbar during analysis. The sample current during analysis ranged from 90 nA to 110 nA. All samples were analysed at an angle of ~20° off normal incident in order to reduce effects from the underlying substrate. Secondary Zn ions were detected using a Hiden Analytical mass spectrometer EQS quadrupole analyser. SIMS measurements were repeated using the benchtop Millbrook miniSIMS alpha system using a positive gallium ion beam at 6 KeV and a quadrupole analyser, with the samples at a 45° angle, as an addition measurement of Zn isotopic distribution in the nanorods. Raman measurements were performed at room temperature using a Horiba LabRAM micro-Raman system. Non-resonant excitation was used to make Raman measurements in the $z(x+y,x+y)\bar{z}$ back-scattering geometry using the 532 nm line of a solid state laser with z-direction coinciding with the direction of the *c*-axis of ZnO.

PL was carried out using a 325 nm HeCd laser as the excitation source directed onto the sample in a Janis model SHI-950-5 cryostat at ~14 K and a diffraction grating

spectrometer system. The spectroscopic system consisted of a 1 m model SPEX 1701 monochromator and Hamamatsu model R3310-02 photomultiplier tube which was cooled to approximately -20 °C. The monochromator contained a grating blazed at 330 nm (ISA model 510-05). A Hg spectral lamp was placed on the optical table such that some of its emission also scattered into the spectrometer entrance slit. The spectral lines from this lamp were used to calibrate the spectra recorded to correct for minor irreproducibility from scan to scan. In addition, the spectra have been corrected for the refractive index of air.

3. RESULTS AND DISCUSSION

3.1. Scanning electron microscopy

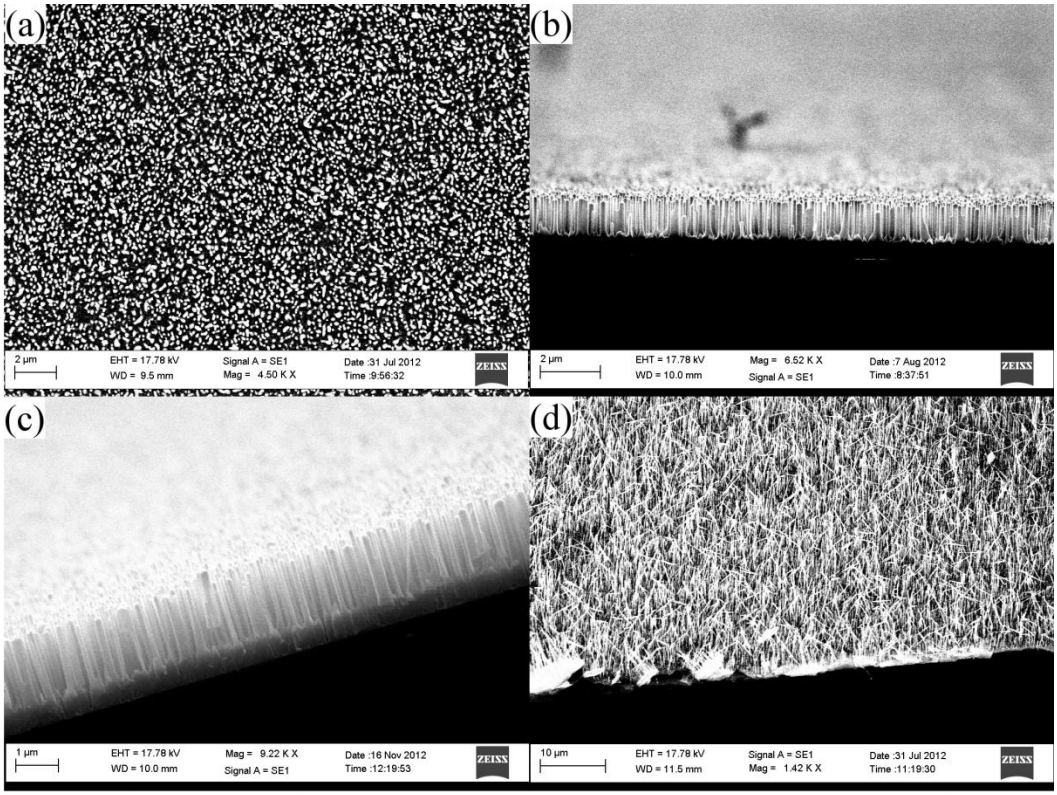

Fig. 1: SEM images showing typical morphology of the ZnO nanorods; (a) plan view of ^{64}ZnO sample; (b) cross-sectional view of ^{64}ZnO sample; (c) cross-sectional view of $^{66/68}$ZnO sample with CBD buffer layer visible; (d) tilted view (at 30° to the vertical) of longer nanorods in ^{66}ZnO sample which have lost vertical alignment and become entangled.

Figure 1 shows SEM images illustrating the morphology of the ZnO nanorod deposits. The silicon substrates in all cases have been covered with a dense pattern of nanorods which are vertically well aligned with their *c*-axes normal to the substrate due to the preferential growth in this direction ultimately caused by the textured seed layer. Coverage of nanorods on the substrates is generally excellent, with good growth occurring over the whole substrate, except for the edges where the sample slightly overhung the edges of the alumina boat which blocked deposition.

Figure 1(a) shows a plan view of the nanorods in a ^{64}ZnO sample. The dense and widespread coverage is clearly observed. These nanorods are shown in cross section in figure 1(b). The cross section is along a freshly cleaved edge through the centre of the sample. The nanorods are approximately 1-2 μm in height, although the variation in a single sample is much smaller than this range. Similar morphology is observed in all other samples. Previous studies carried out in our group investigated the relationship between the nanorod height and diameter.[26] Nanorods of length 1-2 μm typically have diameters of ~100 nm, with shorter nanorods having larger diameters than longer ones. Based on observation of the SEM images shown in this section, the samples in this work appear to fit the patterns identified in these earlier reports. Figure 1(c) shows $^{66/68}$ZnO nanorods, again in cross section. The CBD buffer layer is clearly visible with nanorods growing on the nucleation sites from the buffer layer. Figure 1(d) is taken from a part of the ^{66}ZnO sample. In this case the nanorods are much longer than usual. They have lost their *c*-axis alignment

and have become entangled. Slight variations from the morphology seen here occur from time to time as the growth process is sensitive to a number of parameters including temperature, distance of the sample from the powder, the source powder mixing and particulate size, although in general the batch-to-batch reliability of the growth process is very good.

3.2. X-ray diffraction

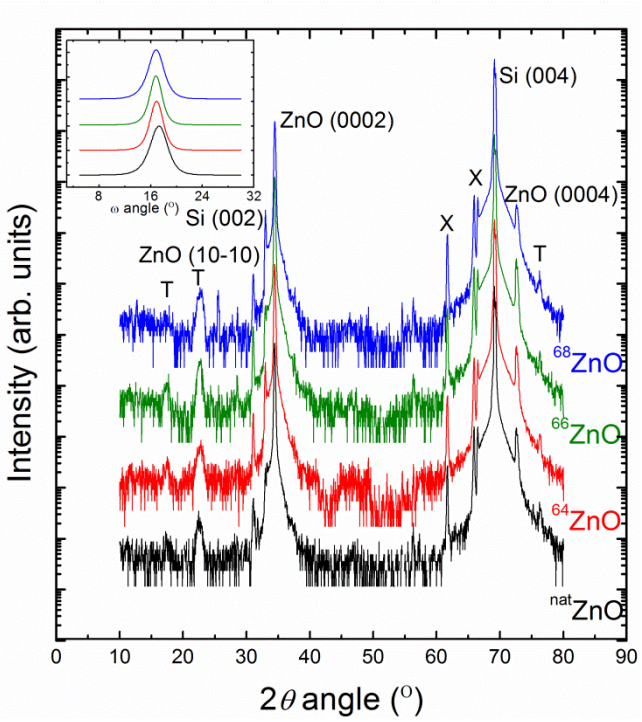

Fig. 2 (color online): 2θ-ω spectra of various ZnO samples showing the dominant Si (004) reflection peak at 69.1° and the ZnO (002) reflection at 34.4°. A number of other features are marked and are described in the text. Inset shows the rocking curves of the 34.4° (0002) ZnO reflection.

Figure 2 shows the XRD 2θ-ω scans for the ^{nat}ZnO, ^{64}ZnO, ^{66}ZnO and ^{68}ZnO samples. These spectra are typical of those obtained from the other samples. The X-ray source was a copper K_α line with an effective mean wavelength of 0.15418 nm. The 2θ-ω spectra are

dominated by the 69.1° silicon peak from the (004) Si planes of the substrate and the 34.4° ZnO peak from the (0002) planes in the deposited ZnO nanorods.[27] The second order (0004) ZnO planes are also present as well as the ZnO (10-10) reflection with a small intensity.[28] The kinematically forbidden Si (002) is also present in some samples due to double diffraction effects.[29] A number of smaller peaks are observed and are attributed to the plastic backed adhesive tape used to mount the samples on the stage. These are labelled as T. A number of features are also visible due to K_β radiation at ~62° from the x-ray tube and tungsten L_α radiation at ~66° from contamination of the x-ray tube Cu target by the electron gun filament.[28] These features are marked as X. The ZnO (0002) is far more intense than the other ZnO reflections, indicating a high degree of alignment of nanostructures with their *c*-axes normal to the substrate surface. The narrow FWHM (~0.20-0.22°) of the 34.4° ZnO peaks indicate that the crystal quality of the nanorods is excellent. These widths imply a coherence length of ~41-47 nm from the Scherrer relation[30] (when the instrumental peak broadening of ~0.10° is taken into account). The XRD data are consistent with the SEM data in figure 1 showing well aligned nanorods. The rocking curves of the 34.4° (0002) ZnO peak from the ^{nat}ZnO, ^{64}ZnO, ^{66}ZnO and ^{68}ZnO samples are shown in the inset in figure 2, and are representative of the other samples (note the linear scale on the inset). The high quality of the crystal structure and *c*-axis alignment shown in SEM images and 2θ-ω scans above is further confirmed by the narrow FWHM of the rocking curves which fall in the range of 2.26-3.25° for all eight samples. The rocking curve peak positions vary slightly due to small variations in sample tilt on the stage, due to the mounting process.[27]

The SEM and XRD data have illustrated that the growth of isotopically enriched ZnO nanorods utilising this three-step process is very successful in terms of sample crystallinity and morphology. This has been achieved by simply substituting the normal, natural isotope

content ZnO source powder used in VPT with isotopically enriched powder and implementing the practical step of reducing the amount of powder used. This easy, reliable and inexpensive method has produced well- aligned nanorods of a very high quality with dense coverage over a wide substrate area. This makes them ideal for use in further optical studies such as Raman and PL.

3.3. SIMS

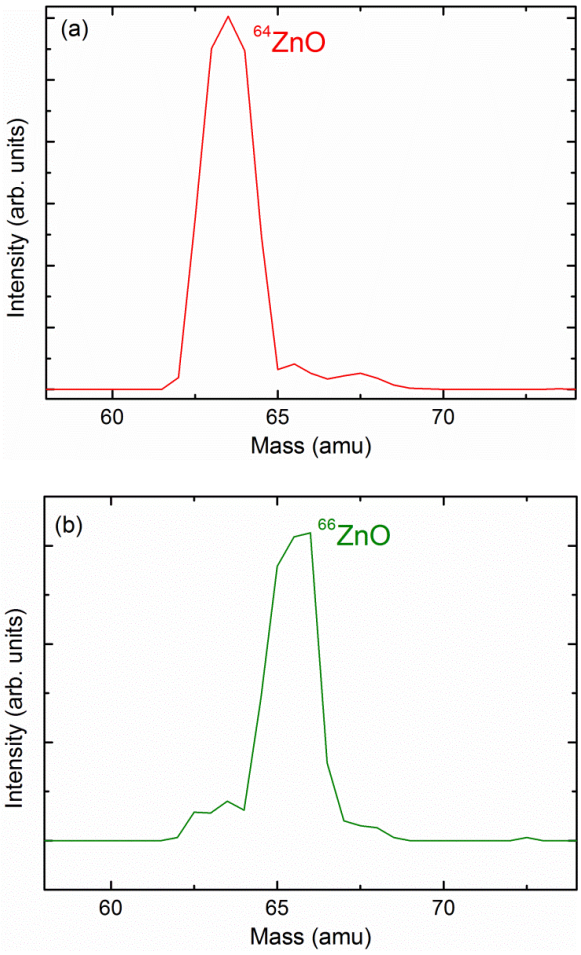

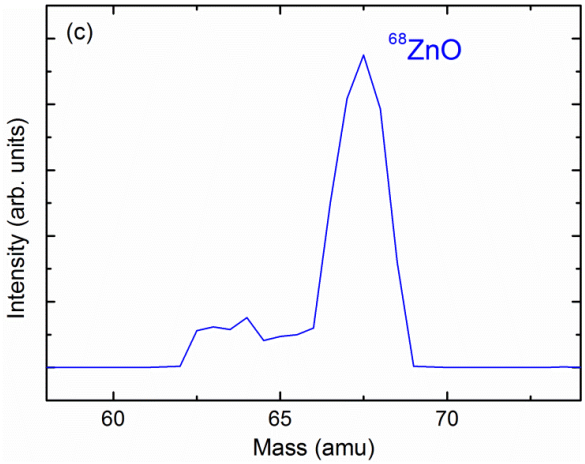

Fig. 3 (color online): SIMS spectra from (a) ^{64}ZnO; (b) ^{66}ZnO; and (c) ^{68}ZnO nanorod samples.

Figure 3 shows representative SIMS spectra for the set from the ^{64}ZnO, ^{66}ZnO and ^{68}ZnO nanorod samples. This provides key evidence as to whether isotopic enrichment has been successful during the growth procedure by measuring the masses of the Zn atoms in the samples. It is clear that the expected Zn isotope is dominant in each respective sample, thereby showing that the samples have been enriched to a very high level. This is of course consistent with the Raman results and PL spectra below. For each enriched isotope, there are smaller peaks at the masses of the other two isotopes. For example, in figure 3(a) for ^{64}ZnO, small peaks are observed at 66 and 68 amu. These small peaks are attributed to some ions of these isotopes arising from the CBD buffer layer, which is not isotopically enriched, and to other ions from any surface contaminants at these masses. The samples were tilted during SIMS measurements, as described above, in order to reduce effects from the underlying substrate, but even with this precaution the VPT nanorod coverage is not complete and a small fraction of the buffer layer is exposed to the ion beam. Despite this, it is clear from the SIMS data that the nanorod samples have been successfully isotopically enriched to a very high level using this growth method. Data obtained the miniSIMS system as a further independent check were consistent with this result.

3.4. Raman spectroscopy

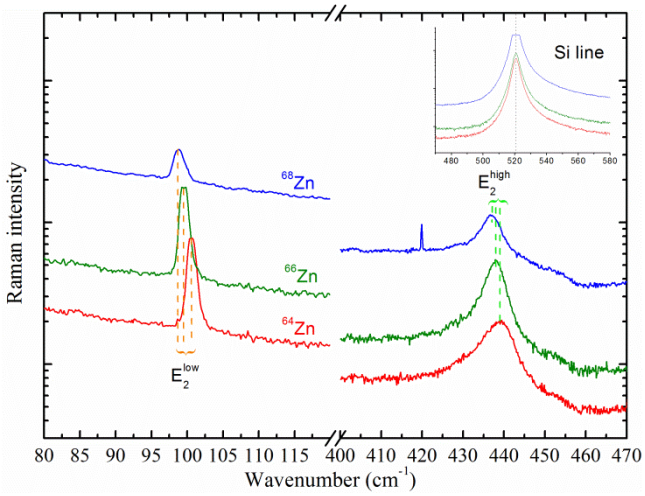

Fig. 4 (color online): Raman spectra of isotopically enriched ^{64}ZnO, ^{66}ZnO and ^{68}ZnO nanorods. Inset shows the signal from the Si substrate.

Sample	**Mode**	**Wavenumber (cm^{-1})**	**ΔWavenumber (cm^{-1})**	**FWHM (cm^{-1})**	**ΔFWHM (cm^{-1})**
^{64}ZnO	E_2^{high}	439.03	-	8.11	-
^{66}ZnO	E_2^{high}	437.73	-1.30	6.94	-1.17
^{68}ZnO	E_2^{high}	436.86	-2.17	5.59	-2.52
^{64}ZnO	E_2^{low}	100.60	-	1.70	-
^{66}ZnO	E_2^{low}	99.57	-1.03	1.70	-0.00
^{68}ZnO	E_2^{low}	98.79	-1.81	1.73	-0.03

Table 1: Frequencies and FWHM of the E_2^{low} and E_2^{high} phonons for ^{64}ZnO, ^{66}ZnO and ^{68}ZnO samples.

Data from Raman spectroscopy measurements performed on ^{64}ZnO, ^{66}ZnO and ^{68}ZnO samples at room temperature are presented in figure 4. In the inset of figure 4, the signal from the underlying Si substrate at around 520 cm^{-1} is shown for reference. For all structures, the Raman spectra contain first-order E_2^{low} and E_2^{high} phonon modes that are typical for crystalline wurtzite ZnO. The two Raman modes gradually shift to lower frequencies with increasing Zn isotope mass from ^{64}ZnO to ^{68}ZnO, by 1.81 cm^{-1} for E_2^{low} and 2.17 cm^{-1} for

E_2^{high}, consistent with previous findings of shifts of 1.59 cm^{-1} for E_2^{high} at low temperatures (~6 K).[31] The frequencies of the E_2^{low} and E_2^{high} phonon modes (100.60 cm^{-1} and 439.03 cm^{-1} respectively for ^{64}ZnO) in each sample and their FWHM are summarized in table 1.

Shifting phonon frequencies for O and Zn isotopic substitution in ZnO have been observed previously in a number of papers by Serrano et al.[22,31] and are observed here for the E_2^{high} and E_2^{low} phonon modes. Since only the natural abundance of O (>99% ^{16}O) was used during nanorod growth in this work the changing Zn mass is solely responsible for the shifting phonon frequencies. For the E_2^{high} phonon mode the observed frequency change for different Zn masses (around 2 cm^{-1}) is less pronounced than that for different O masses (around 20 cm^{-1}) due to the dominating O eigenvector.[22] A similar shift (<2 cm^{-1}) is observed for the E_2^{low} phonon with changing Zn mass.

However, the significant broadening of the FWHM for the E_2^{high} mode is not isotopic in nature. The changing FWHM for different Zn masses results from a change in the overlap of the two-phonon density of states due to changes in phonon frequency. Ab initio calculations performed by Serrano et al.[22] show that the E_2^{high} phonon mode is near a sharp 'ridge' in the two-phonon density of states, the interaction with which results in the variation in FWHM. The overlap is less clearly observed for the E_2^{low} mode with no change observed in the FWHM with changing Zn mass. Our data are consistent with the results reported by Serrano et al.

The observed shifts in the phonon vibration energies in our samples follow estimates based on the harmonic oscillator approach, are consistent with previous findings in the literature and, therefore, demonstrate clearly, and independently of the SIMS data above and the PL experiments below, that the desired isotopic enrichment of the samples has been successful.

3.5. Low temperature photoluminescence

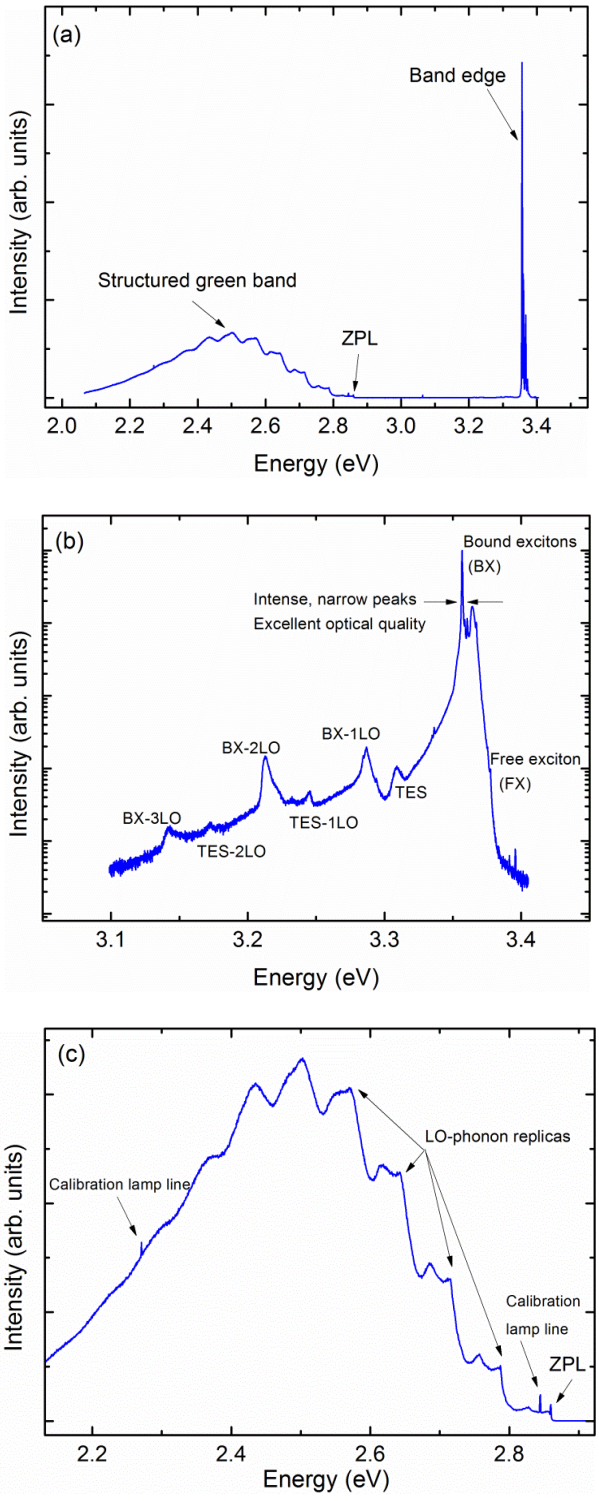

Fig. 5 (color online): PL spectra of the ^{66}ZnO sample taken at ~14 K showing (a) a broad range spectrum displaying the typical PL emission from ZnO nanorods, (b) the intense UV band edge emission in detail, and (c) the Cu-related 2.86 eV ZPL and associated structured green band (from annealed portion). (Note that (a) is a composite of (b) and (c)).

Low temperature PL was carried out on all samples. Figure 5(a) shows a broad spectrum including the band edge region, as well as the Cu-related zero phonon line (ZPL) at 2.86 eV and its associated structured green band in ^{66}ZnO (note the linear y-scale here).[32,33] ^{66}ZnO was chosen to illustrate the general features of these spectra as its spectrum was representative of those obtained from the other samples and typical of the PL spectrum obtained from ZnO nanorods reported in the literature.[34] Note that figure 5(a) is a composite of the spectra in figures 5(b) and (c) in order to show a broad spectrum.

Figure 5(b) shows the band edge region of the ^{66}ZnO sample in detail (note the logarithmic y-scale). The intense band edge emission due to shallow donor bound excitons (BX) is dominant at ~3.36 eV. The free exciton (FX) position can also be seen, although this was not clearly observed in all samples. The longitudinal optical (LO) phonon replicas of the bound excitons are also present (BX-1LO, BX-2LO and BX-3LO), spaced at intervals of ~72 meV, the characteristic LO phonon energy of the ZnO crystal structure.[35] The two electron satellite (TES) feature is also present, as are its LO replicas (TES-1LO and TES-2LO). The intense peaks and narrow line widths (<1 meV) of the BX lines indicate the excellent optical quality of the nanorods as grown, as discussed further below. This is consistent with the excellent optical characteristics of ZnO nanorods grown by similar methods reported elsewhere and demonstrates the ability to grow isotopically enriched ZnO materials with excellent optical quality using the straightforward carbothermal reduction VPT method, with mg quantities of source material.[36] Note that the PL emission is associated with the VPT-grown nanorods and there is not a significant emission from the underlying buffer layer.[37]

Figure 5(c) shows the green band emission region for ^{66}ZnO. This was recorded using a portion of the ^{66}ZnO sample which was annealed for ten minutes at 900 °C to increase the ZPL and green band intensity.[36,38] The Cu-related ZPL at 2.86 eV is present and its

associated structured green band is the dominant feature. Indeed, the structured green band is the primary feature of the PL spectrum in addition to the UV band edge emission. The LO-phonon replicas of the ZPL are clearly seen in the structured green band at intervals of ~72 meV below the ZPL energy. Some weak lines from the Hg lamp used to calibrate the spectra are also observed.

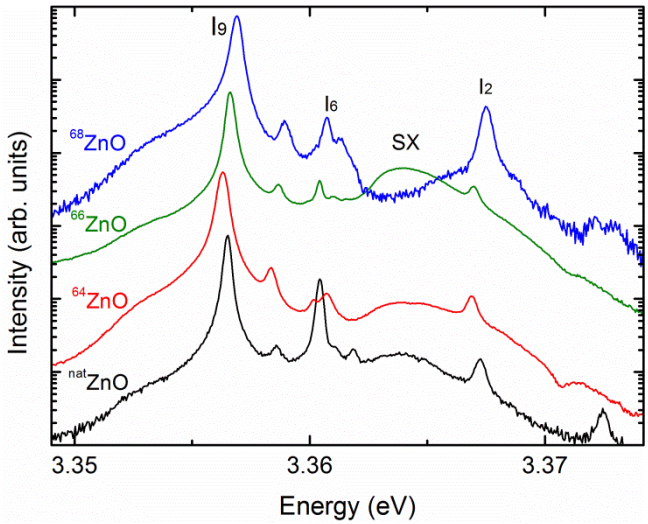

Fig. 6 (color online): Typical PL spectra of selected enriched ZnO nanorod samples showing the band edge region including the I_9 line (~14 K, spectra shifted vertically for clarity).

Sample	**Average Zn isotopic content (amu)**	**I_9 energy (eV)**	**I_9 FWHM (meV)**
^{64}ZnO	64	3.35629	0.44
^{66}ZnO	66	3.35662	0.36
^{68}ZnO	68	3.35689	0.41
$^{64/66}$ZnO	65	3.35641	0.33
$^{66/68}$ZnO	67	3.35682	0.33
$^{64/68}$ZnO	66	3.35643	0.35
$^{64/66/68}$ZnO	66	3.35603	0.35
^{nat}ZnO	65.4	3.3565	0.31

Table 2: Energies and FWHM of the I_9 exciton recombination in samples with different Zn isotopes.

Figure 6 shows representative band edge spectra from selected samples. The dominant feature in the band edge spectra is the I_9 line attributed to indium[39] donor bound impurities. The I_6 line attributed to aluminium impurities is also clearly observed.[40,41] The I_2 line attributed to ionised indium impurities[42] and the surface exciton[43] (SX) emission are also visible and labelled in the figure.

The position of the I_9 indium bound exciton recombination in unenriched material at ~3.356 eV was used to measure changes in the band edge positions with changing Zn isotope enrichment. The peak positions of the I_9 line were extracted by fitting Gaussian curves to the data. The position of the I_9 line in each sample is given in table 2, along with their FWHM. The I_9 bound exciton energy increases with increasing Zn isotopic mass from ^{64}ZnO to ^{68}ZnO by 0.6 meV. The blue shift in energy recorded in the band edge region when the Zn isotope mass is changed (0.6 meV) is comparable to that previously reported in the literature. Tsoi et al. report an increase of ~1.0 meV in the A-exciton band gap over this range.[21] This is further verification of the successful isotopic enrichment of our samples. We note that Manjón et al. report blue shifts in the band edge region of ~1.7 meV from ^{64}ZnO to ^{68}ZnO for single crystals.[20] However since Manjón at al.'s results come from measurements of the I_4 bound exciton recombination and since this emission has been attributed to hydrogen at an oxygen site[44] (i.e. a hydrogen atom surrounded by Zn atoms), this recombination may be more strongly affected by Zn isotopic changes (due to both local and extended vibronic modes) and undergo a different shift than other shallow donor bound excitons on Zn sites surrounded by O atoms (such as the In-related I_9).

The very narrow FWHM of the exciton recombinations in these nanorod samples demonstrates their excellent optical quality and therefore their suitability for use in defect and impurity studies using PL. The I_9 FWHMs here are in the range of 0.31-0.44 meV as shown in table 2 (comparable to very high optical quality commercial single crystal ZnO[42]). This

is much narrower than the line widths observed by others in single crystal isotopically enriched ZnO. Manjón et al. have reported line widths of < 5 meV[20] and Tsoi et al. observed BX PL features of widths of ~2-8 meV[21] in single crystal isotopically enriched ZnO samples. Given this excellent optical quality, we intend on using these samples to carry out a number of detailed optical studies of defects in ZnO, including the Cu-related emission ZPL at 2.86 eV, as well as the manifold of closely spaced near band edge I lines due to donor bound exciton emission.

4. CONCLUSION

The three-step growth process previously developed in our group, has been successfully adapted in order to grow nanorods of ZnO isotopically enriched with different Zn isotopes. Samples of ^{nat}ZnO, ^{64}ZnO, ^{66}ZnO, ^{68}ZnO, $^{64/66}$ZnO, $^{66/68}$ZnO, $^{64/68}$ZnO and $^{64/66/68}$ZnO were grown. SEM revealed a dense coverage of vertical, *c*-axis aligned nanorods over a large sample area for nearly all samples, with slight variations seen in one sample. XRD confirmed the presence of ZnO and the excellent nanorod alignment and crystal quality. SIMS data confirm the successful isotopic enrichment. Raman data show a shift of >1 cm^{-1} in the peak position of the Raman scattered peaks due to the E_2^{low} and E_2^{high} phonon modes when the Zn isotope is changed from ^{64}Zn to ^{68}Zn, consistent with previous work on samples with different isotopic enrichments, again confirming successful isotopic substitution.

Low temperature PL measurements revealed the excellent optical quality of the samples with an increase in the I_9 position of ~0.6 meV with Zn isotopic content changes from ^{64}ZnO to ^{68}ZnO and narrow line widths of <1 meV. This is consistent with previous results reported for single crystals, further confirming successful isotopic substitution of these high structural and optical quality nanorods using this simple and reliable growth method.

The excellent optical quality also suggests possible applications for defect and impurity studies using PL.

ACKNOWLEDGEMENTS

CG and EMcG gratefully acknowledge the Irish Research Council (IRC) for a postgraduate scholarship under the EMBARK initiative. CG acknowledges invaluable support from Dr. Daragh Byrne.

REFERENCES

[1] D. Bao, H. Gu, A. Kuang, Sol-gel-derived c-axis oriented ZnO thin films, Thin Solid Films. 312 (1997) 37–39. doi:10.1016/S0040-6090(97)00302-7.

[2] L.E. Greene, M. Law, D.H. Tan, M. Montano, J. Goldberger, G. Somorjai, et al., General Route to Vertical ZnO Nanowire Arrays Using Textured ZnO Seeds, Nano Lett. 5 (2005) 1231–1236. doi:10.1021/nl050788p.

[3] D. Byrne, E. McGlynn, K. Kumar, M. Biswas, M.O. Henry, G. Hughes, A Study of Drop-Coated and Chemical Bath-Deposited Buffer Layers for Vapor Phase Deposition of Large Area, Aligned, Zinc Oxide Nanorod Arrays, Cryst. Growth Des. 10 (2010) 2400–2408. doi:10.1021/cg100231u.

[4] S.H. Jo, J.Y. Lao, Z.F. Ren, R. a. Farrer, T. Baldacchini, J.T. Fourkas, Field-emission studies on thin films of zinc oxide nanowires, Appl. Phys. Lett. 83 (2003) 4821. doi:10.1063/1.1631735.

[5] M. Law, L.E. Greene, J.C. Johnson, R. Saykally, P. Yang, Nanowire dye-sensitized solar cells., Nat. Mater. 4 (2005) 455–9. doi:10.1038/nmat1387.

[6] J. Grabowska, a. Meaney, K. Nanda, J.-P. Mosnier, M. Henry, J.-R. Duclère, et al., Surface excitonic emission and quenching effects in ZnO nanowire/nanowall systems: Limiting effects on device potential, Phys. Rev. B. 71 (2005) 115439. doi:10.1103/PhysRevB.71.115439.

[7] T. Long, S. Yin, K. Takabatake, P. Zhnag, T. Sato, Synthesis and Characterization of ZnO Nanorods and Nanodisks from Zinc Chloride Aqueous Solution., Nanoscale Res. Lett. 4 (2009) 247–253. doi:10.1007/s11671-008-9233-2.

[8] X.Y. Kong, Z.L. Wang, Spontaneous Polarization-Induced Nanohelixes, Nanosprings, and Nanorings of Piezoelectric Nanobelts, Nano Lett. 3 (2003) 1625–1631. doi:10.1021/nl034463p.

[9] Y. Wang, X. Chen, J. Zhang, Z. Sun, Y. Li, K. Zhang, et al., Fabrication of surface-patterned and free-standing ZnO nanobowls, Colloids Surfaces A Physicochem. Eng. Asp. 329 (2008) 184–189. doi:10.1016/j.colsurfa.2008.07.018.

[10] K. Govender, D.S. Boyle, P.B. Kenway, P.O. Brien, Understanding the factors that govern the deposition and morphology of thin films of ZnO from aqueous solution, J. Mater. Chem. 14 (2004) 2575–2591.

[11] J. Grabowska, K.K. Nanda, E. McGlynn, J.-P. Mosnier, M.O. Henry, Studying the growth conditions, the alignment and structure of ZnO nanorods, Surf. Coatings Technol. 200 (2005) 1093–1096. doi:10.1016/j.surfcoat.2005.01.030.

[12] D.J. Park, D.C. Kim, J.Y. Lee, H.K. Cho, Synthesis and microstructural characterization of growth direction controlled ZnO nanorods using a buffer layer, Nanotechnology. 17 (2006) 5238–5243. doi:10.1088/0957-4484/17/20/032.

[13] H. Xu, H. Wang, Y. Zhang, W. He, M. Zhu, B. Wang, et al., Hydrothermal synthesis of zinc oxide powders with controllable morphology, Ceram. Int. 30 (2004) 93–97. doi:10.1016/S0272-8842(03)00069-5.

[14] G. Davies, E.C. Lightowlers, R. Woolley, R.C. Newman, a S. Oates, Carbon in radiation damage centres in Czochralski silicon, J. Phys. C Solid State Phys. 17 (1984) L499–L503. doi:10.1088/0022-3719/17/19/005.

[15] M.L.W. Thewalt, Spectroscopy of excitons and shallow impurities in isotopically enriched silicon—electronic properties beyond the virtual crystal approximation, Solid State Commun. 133 (2005) 715–725. doi:10.1016/j.ssc.2004.12.023.

[16] D. Barba, D. Koshel, F. Martin, G.G. Ross, M. Chicoine, F. Schiettekatte, et al., Silicon nanocrystal synthesis by implantation of natural Si isotopes, J. Lumin. 130 (2010) 669–673. doi:10.1016/j.jlumin.2009.11.014.

[17] F.J. Manjón, M. a. Hernández-Fenollosa, B. Marí, S.F. Li, C.D. Poweleit, a. Bell, et al., Effect of N isotopic mass on the photoluminescence and cathodoluminescence spectra of gallium nitride, Eur. Phys. J. B. 40 (2004) 453–458. doi:10.1140/epjb/e2004-00211-1.

[18] J.M. Zhang, T. Ruf, M. Cardona, O. Ambacher, M. Stutzmann, J.-M. Wagner, et al., Raman spectra of isotopic GaN, Phys. Rev. B. 56 (1997) 14399. doi:10.1103/PhysRevB.56.14399.

[19] T.. Meyer, D. Karaiskaj, M.L.. Thewalt, M. Cardona, Effect of the isotopic mass of gallium on the indirect gap of GaP, Solid State Commun. 126 (2003) 119–123. doi:10.1016/S0038-1098(03)00030-9.

[20] F.J. Manjón, M. Mollar, M.A. Hernández-Fenollosa, B. Marí, R. Lauck, M. Cardona, Effect of isotopic mass on the photoluminescence spectra of zinc oxide, Solid State Commun. 128 (2003) 35–39. doi:10.1016/S0038-1098(03)00616-1.

[21] S. Tsoi, X. Lu, a. Ramdas, H. Alawadhi, M. Grimsditch, M. Cardona, et al., Isotopic-mass dependence of the A, B, and C excitonic band gaps in ZnO at low temperatures, Phys. Rev. B. 74 (2006) 165203. doi:10.1103/PhysRevB.74.165203.

[22] J. Serrano, F. Manjón, a. Romero, F. Widulle, R. Lauck, M. Cardona, Dispersive Phonon Linewidths: The E2 Phonons of ZnO, Phys. Rev. Lett. 90 (2003) 055510. doi:10.1103/PhysRevLett.90.055510.

[23] J. Serrano, R. Kremer, M. Cardona, G. Siegle, a. Romero, R. Lauck, Heat capacity of ZnO: Isotope effects, Phys. Rev. B. 73 (2006) 094303. doi:10.1103/PhysRevB.73.094303.

[24] M. Biswas, E. McGlynn, M.O. Henry, M. McCann, a. Rafferty, Carbothermal reduction vapor phase transport growth of ZnO nanostructures: Effects of various carbon sources, J. Appl. Phys. 105 (2009) 094306. doi:10.1063/1.3121213.

[25] R.B. Peterson, C.L. Fields, B.A. Gregg, Epitaxial Chemical Deposition of ZnO Nanocolumns from NaOH Solutions, Langmuir. 20 (2004) 5114–5118. doi:10.1021/la049683c.

[26] R.B. Saunders, S. Garry, D. Byrne, M.O. Henry, E. McGlynn, Length versus Radius Relationship for ZnO Nanowires Grown via Vapor Phase Transport, Cryst. Growth Des. 12 (2012) 5972–5979. doi:10.1021/cg3009738.

[27] E. McCarthy, R.T. Rajendra Kumar, B. Doggett, S. Chakrabarti, R.J. O'Haire, S.B. Newcomb, et al., Effects of the crystallite mosaic spread on integrated peak intensities in 2θ–ω measurements of highly crystallographically textured ZnO thin films, J. Phys. D. Appl. Phys. 44 (2011) 375401. doi:10.1088/0022-3727/44/37/375401.

[28] R.T.R. Kumar, E. McGlynn, M. Biswas, R. Saunders, G. Trolliard, B. Soulestin, et al., Growth of ZnO nanostructures on Au-coated Si: Influence of growth temperature on growth mechanism and morphology, J. Appl. Phys. 104 (2008) 084309. doi:10.1063/1.2996279.

[29] B.-H. Hwang, Calculation and measurement of all (002) multiple diffraction peaks from a (001) silicon wafer, J. Phys. D. Appl. Phys. 34 (2001) 2469–2474. doi:10.1088/0022-3727/34/16/311.

[30] V. Mote, Y. Purushotham, B. Dole, Williamson-Hall analysis in estimation of lattice strain in nanometer-sized ZnO particles, J. Theor. Appl. Phys. 6 (2012) 6. doi:10.1186/2251-7235-6-6.

[31] J. Serrano, F. Widulle, A.H. Romero, A. Rubio, R. Lauck, M. Cardona, Dependence of phonon widths on pressure and isotopic mass : ZnO, Phys. Status Solidi. 235 (2003) 260–266. doi:10.1002/pssb.200321566.

[32] R. Dingle, Luminescent transitions associated with divalent copper impurties and the green emission from semiconducting zinc oxide, Phys. Rev. Lett. 23 (1969) 579–581.

[33] D. Byrne, F. Herklotz, M.O. Henry, E. McGlynn, Unambiguous identification of the role of a single Cu atom in the ZnO structured green band, J. Physics. Condens. Matter. 24 (2012) 215802. doi:10.1088/0953-8984/24/21/215802.

[34] C.F. Klingshirn, B.K. Meyer, A. Waag, A. Hoffmann, J. Geurts, ZnO: From Fundamental Properties Towards Novel Applications, Springer-Verlag, Berlin, Heidelberg, 2010. doi:10.1007/978-3-642-10577-7.

[35] L. Wang, N.C. Giles, Temperature dependence of the free-exciton transition energy in zinc oxide by photoluminescence excitation spectroscopy, J. Appl. Phys. 94 (2003) 973. doi:10.1063/1.1586977.

[36] G. Xing, G. Xing, M. Li, E.J. Sie, D. Wang, A. Sulistio, et al., Charge transfer dynamics in Cu-doped ZnO nanowires, Appl. Phys. Lett. 98 (2011) 102105. doi:10.1063/1.3558912.

[37] D. Byrne, E. McGlynn, J. Cullen, M.O. Henry, A catalyst-free and facile route to periodically ordered and c-axis aligned ZnO nanorod arrays on diverse substrates, Nanoscale. 3 (2011) 1675–82. doi:10.1039/c0nr00919a.

[38] N.Y. Garces, L. Wang, L. Bai, N.C. Giles, L.E. Halliburton, G. Cantwell, Role of copper in the green luminescence from ZnO crystals, Appl. Phys. Lett. 81 (2002) 622. doi:10.1063/1.1494125.

[39] S. Müller, D. Stichtenoth, M. Uhrmacher, H. Hofsäss, C. Ronning, J. Röder, Unambiguous identification of the PL-I[sub 9] line in zinc oxide, Appl. Phys. Lett. 90 (2007) 012107. doi:10.1063/1.2430483.

[40] M. Schilling, R. Helbig, G. Pensl, Bound exciton luminescence of Ar- and Al-implanted ZnO, J. Lumin. 33 (1985) 201–212. doi:10.1016/0022-2313(85)90018-3.

[41] B.K. Meyer, H. Alves, D.M. Hofmann, W. Kriegseis, D. Forster, F. Bertram, et al., Bound exciton and donor–acceptor pair recombinations in ZnO, Phys. Status Solidi. 241 (2004) 231–260. doi:10.1002/pssb.200301962.

[42] J. Cullen, D. Byrne, K. Johnston, E. McGlynn, M.O. Henry, Chemical identification of luminescence due to Sn and Sb in ZnO, Appl. Phys. Lett. 102 (2013) 192110. doi:10.1063/1.4807288.

[43] M. Biswas, Y.S. Jung, H.K. Kim, K. Kumar, G.J. Hughes, S. Newcomb, et al., Microscopic origins of the surface exciton photoluminescence peak in ZnO nanostructures, Phys. Rev. B. 83 (2011) 235320. doi:10.1103/PhysRevB.83.235320.

[44] E. Lavrov, F. Herklotz, J. Weber, Identification of two hydrogen donors in ZnO, Phys. Rev. B. 79 (2009) 165210. doi:10.1103/PhysRevB.79.165210.

Growth of isotopically enriched ZnO nanorods of excellent optical quality

Ciarán Gray[1,*], Joseph Cullen[2], Conor Byrne[3], Greg Hughes[3], Irina Buyanova[2], Weimin Chen[2], Martin O. Henry[1], Enda McGlynn[1,*]

[1] *School of Physical Sciences, National Centre for Plasma Science and Technology, Dublin City University, Glasnevin, Dublin 9, Ireland.*

[2] *Department of Physics, Chemistry and Biology, Linköping University, S-581 83, Linköping, Sweden.*

[3] *School of Physical Sciences, Dublin City University, Glasnevin, Dublin 9, Ireland.*

*Authors to whom correspondence should be addressed: ciaran.gray5@mail.dcu.ie (Ph. 0035317007695), enda.mcglynn@dcu.ie.

BLACK AND WHITE VERSIONS OF FIGURES IN MANUSCRIPT FILE

Figure 1:

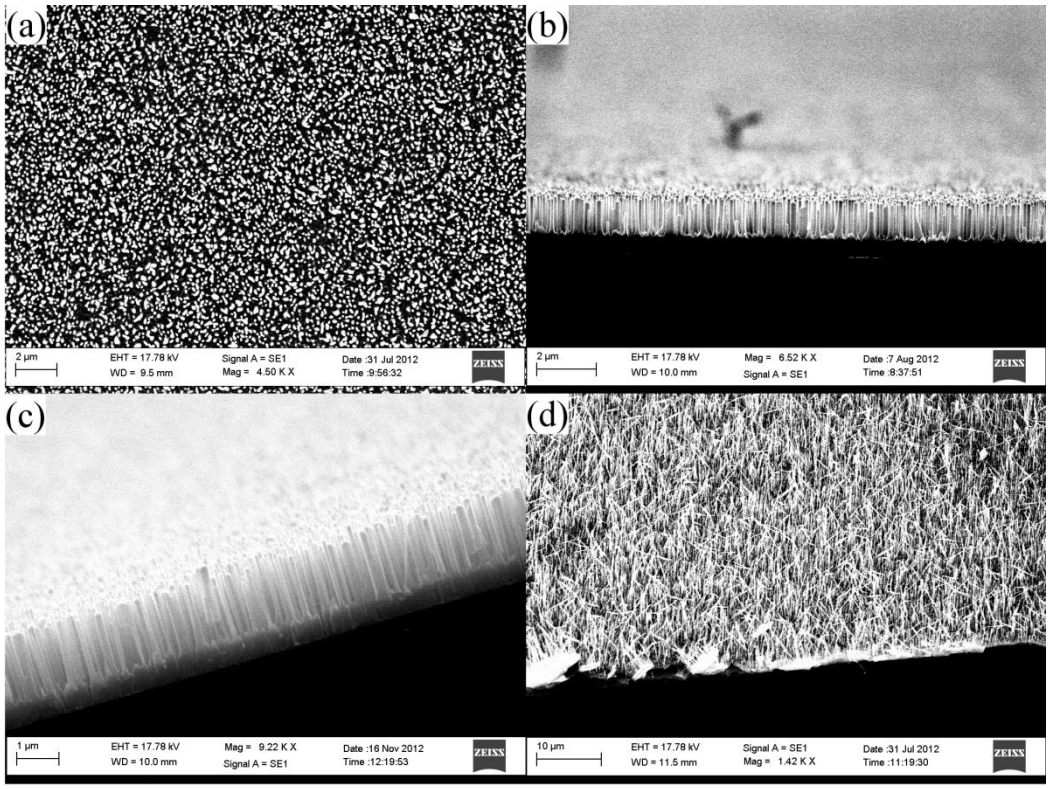

Figure 2:

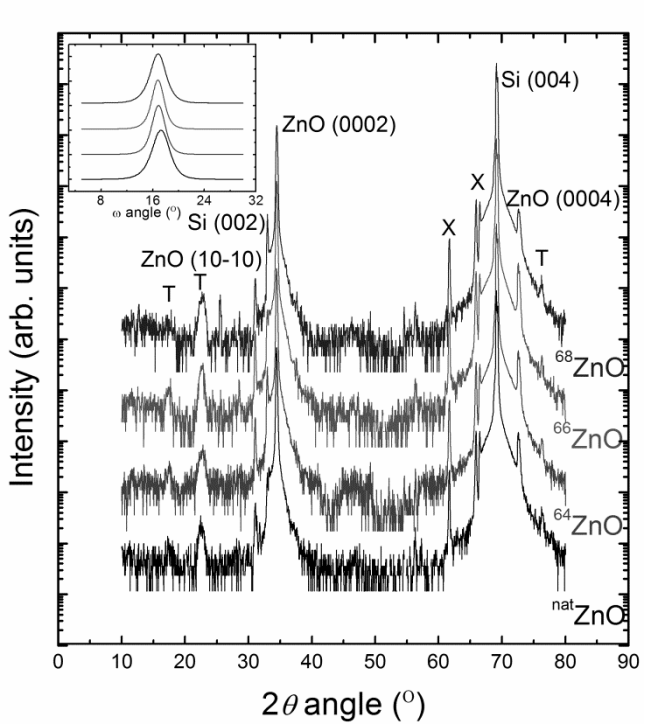

Figure 3:

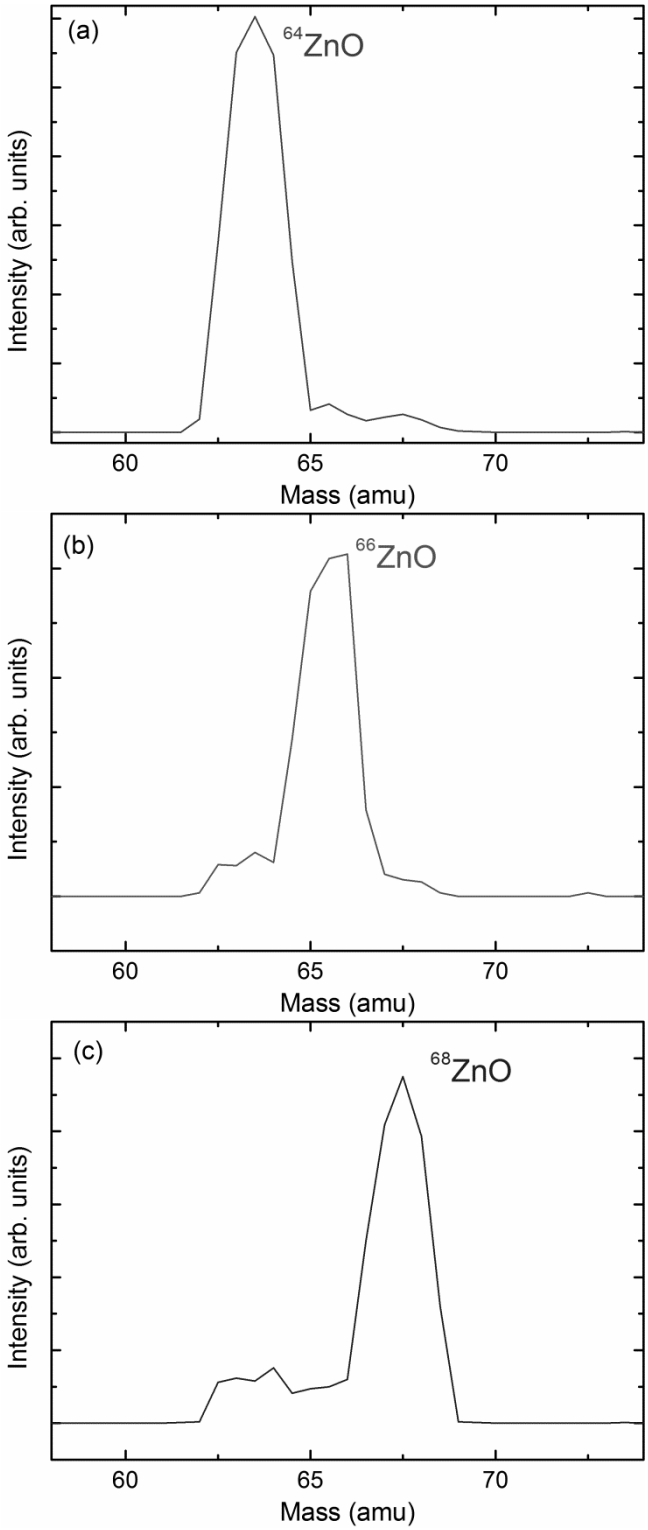
(a)
^{64}ZnO
Intensity (arb. units)
60
65
70
Mass (amu)
(b)
^{66}ZnO
Intensity (arb. units)
60
65
70
Mass (amu)
(c)
^{68}ZnO
Intensity (arb. units)
60
65
70
Mass (amu)

Figure 4:

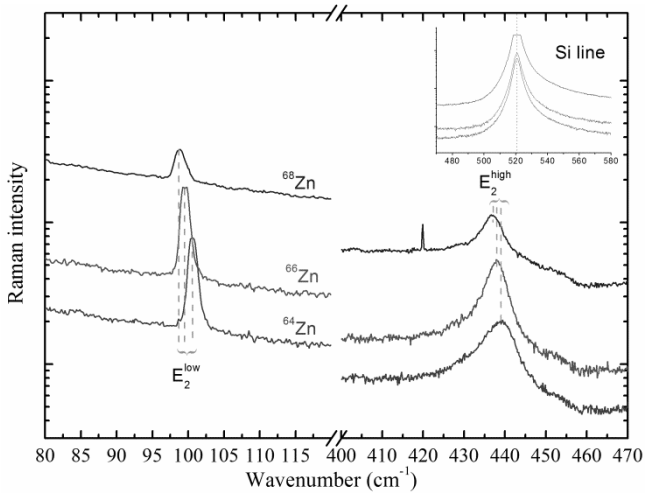
Raman intensity
^{68}Zn
^{66}Zn
^{64}Zn
E_2^{low}
E_2^{high}
Si line
480 500 520 540 560 580
80 85 90 95 100 105 110 115 400 410 420 430 440 450 460 470
Wavenumber (cm^{-1})

Figure 5:

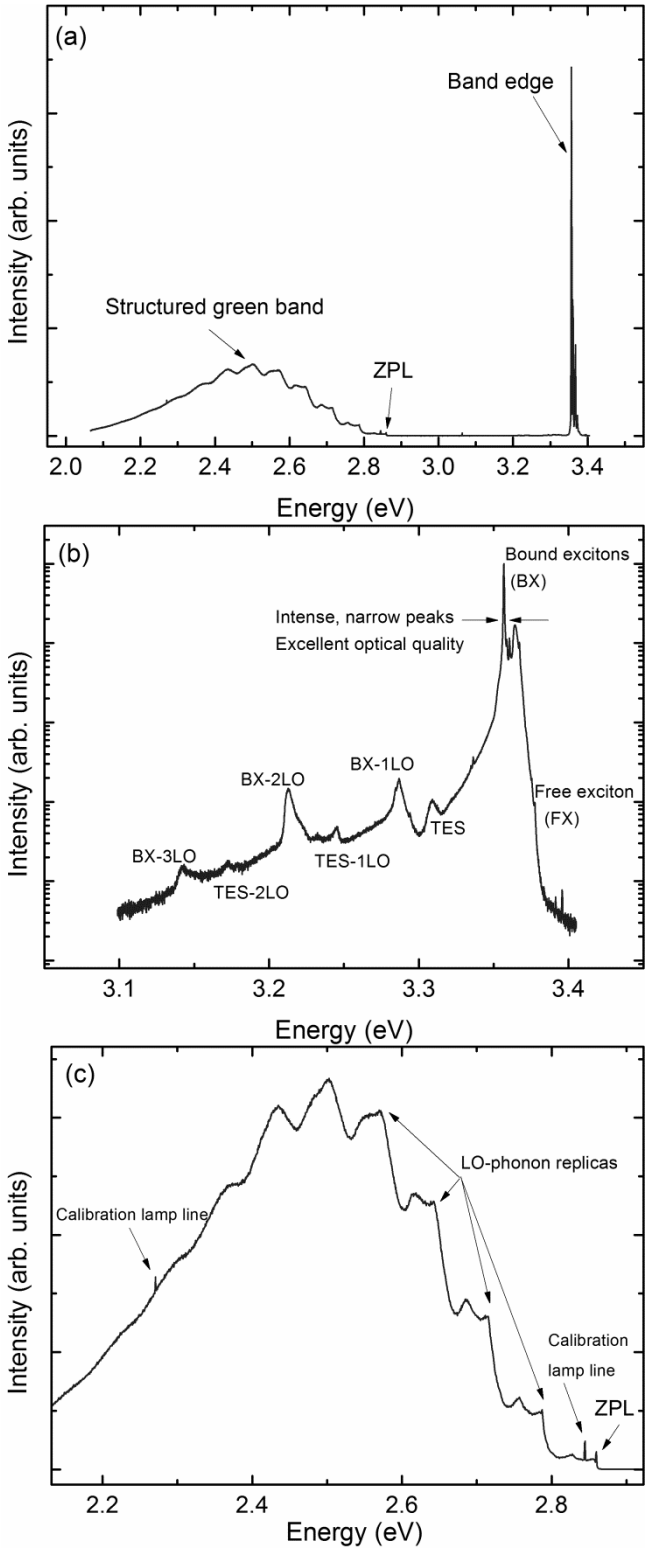
(a)
Band edge
Structured green band
ZPL
Intensity (arb. units)
2.0
2.2
2.4
2.6
2.8
3.0
3.2
3.4
Energy (eV)
(b)
Bound excitons
(BX)
Intense, narrow peaks
Excellent optical quality
BX-2LO
BX-1LO
Free exciton
(FX)
TES
BX-3LO
TES-1LO
TES-2LO
Intensity (arb. units)
3.1
3.2
3.3
3.4
Energy (eV)
(c)
LO-phonon replicas
Calibration lamp line
Calibration
lamp line
ZPL
Intensity (arb. units)
2.2
2.4
2.6
2.8
Energy (eV)

Figure 6:

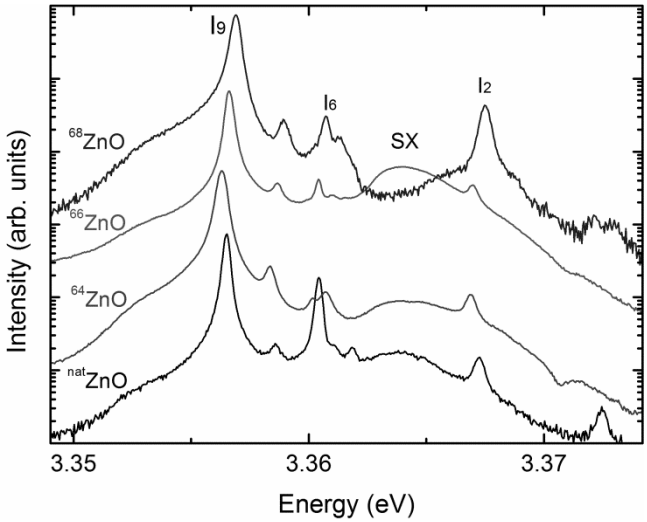
I9
I6
I2
SX
68ZnO
66ZnO
64ZnO
natZnO
Intensity (arb. units)
3.35
3.36
3.37
Energy (eV)